

Systematics of g factor in even-even rare earth nuclei: A microscopic description by the triaxial projected shell model

Bao-An Bian¹, Yao-Min Di¹, Gui-Lu Long^{2,1}, Yang Sun^{3,1}, Javid A. Sheikh⁴

¹*Department of Physics, Xuzhou Normal University, Xuzhou, Jiangsu 221009, P.R. China*

²*Department of Physics, Tsinghua University, Beijing 100084, P.R. China*

³*Department of Physics and Joint Institute for Nuclear Astrophysics,
University of Notre Dame, Notre Dame, Indiana 46556, USA*

⁴*Department of Physics, University of Kashmir, Hazratbal, Srinagar, Kashmir 190 006, India*

(Dated: May 24, 2019)

The systematics of g factor of first excited 2^+ state in the rare earth region is studied by the triaxial projected shell model. The study covers the even-even nuclei of all the isotopic chains from Gd to Pt. g factors are calculated by using the wave-functions obtained from a shell-model diagonalization that reproduces well the ground-state bands and γ -vibrational bands. For Gd to W nuclei the characteristic feature of the g factor data along an isotopic chain is consistently described by the present model. Deficiency of the model in the g factor description for the heavier Os and Pt isotopes is discussed.

PACS numbers: 21.10.Re, 21.60.Cs, 24.10.Cn, 27.60.+j

I. INTRODUCTION

Nuclear magnetic dipole moment can provide valuable information on the microscopic structure of a nuclear system. It is a sensitive probe of nuclear wave-functions, and hence can serve as a strict testing ground for theoretical models. Because of the intrinsically opposite signs of the neutron and proton g_s , a study of gyromagnetic factor (g factor) enables determination of the detailed structure for underlying states. For example, variation of g factors often is a clear indicator for a single-particle component that strongly influences the total wave-function. With advances in modern experimental techniques and sensitive detectors, progress in the g factor measurement has continuously been made. In a recent paper [1], Berant *et al.*, by summarizing their new and the accumulated data from Refs. [2, 3], raised an interesting question on the systematic behavior of the 2^+ g factors in the rare earth region. For even-even nuclei, the current set of data indicates the characteristic feature of the systematics (see Fig. 2 below): with increasing neutron number, the 2^+ g factors display a decreasing trend in the Gd, Dy, and Er isotopes; stay nearly constant within a range of the Yb and Hf chains; then change to an increasing trend in the W and Os isotopes; but show a flat behavior in the Pt chain.

Clearly, the overall behavior of these 2^+ g factors exhibits a large deviation from the rotor value, Z/A , which has only a very weak and smooth dependence on nucleon numbers [4]. On the other hand, the proton-neutron version of the interacting boson model [5] gives a too strong particle number dependence, and thus fails to reproduce the flat behavior of the g factors near the midshells [1]. These facts may suggest that in realistic nuclear systems, g factors reflect a delicate interplay of collective and single-particle degrees of freedom, which is dictated by the detailed shell structure. Simple, phenomenological models do not sufficiently provide such information. It is thus desired that the g factor systematics can be understood by microscopic theories. Spherical shell model calculation is applicable only to nuclei near the shell closures (for a recent example, see Ref. [6]). There have been microscopic models employed in the g factor calculation for heavy, deformed nuclei [7, 8, 9, 10, 11, 12, 13]. However, except in Ref. [10], these calculations focused mainly on one or a few chosen examples in an isotopic chain. A systematical microscopic description of the experimental g factor data for an entire mass region has been a challenge to microscopic theories.

In the present work, we attempt to make a systematical microscopic study for 2^+ g factors in the rare earth region. As the theoretical tool, we employ the recently developed code for g factor calculations [14], which is based on the triaxial projected shell model (TPSM) [15]. The calculation will be performed for nuclei from the Gd ($Z = 64$) to the Pt ($Z = 78$) isotopic chains, with neutron numbers ranging from $N = 88$ to 120. These nuclei are known to have very different collective properties, including those of the well-deformed, the γ -soft, and possibly the γ -deformed. For this large group of nuclei, it is therefore not appropriate to apply the projected shell model (PSM) [16], which assumes an axial symmetry in the shell-model basis states. Instead, in the TPSM approach [15], one introduces triaxiality in the deformed basis and performs exactly three-dimensional angular-momentum projection. In this way, the basis states are much enriched by allowing all possible K -components, and this equivalently enlarges the Hilbert space of the original PSM. Diagonalization mixes these K -states, and besides the $K = 0$ ground-state band (g-band), various collectively excited levels naturally emerge [17]. In the TPSM, the first excited band describes the observed γ -vibrational band, and the second excited one accounts for the experimental $\gamma\gamma$ -band. The TPSM has also been successfully applied to the study of transition quadrupole moments in the g-band and γ -vibrational band for γ -soft

nuclei [18], and to the study of inter-band BE(2) values connecting these bands [19]. These achievements let us to believe that the TPSM, which is a realistic quantum-mechanical model and has been successful in various studies of nuclear properties, is a proper microscopic theory for the present investigation.

II. OUTLINE OF THE THEORY

Shell-model diagonalization in the TPSM provides well-defined wave-functions, $|\Psi_{IM}^\sigma\rangle$, written in the laboratory frame. g factors can then be directly computed as

$$g(\sigma, I) = \frac{\mu(\sigma, I)}{\mu_N I} = \frac{1}{\mu_N I} [\mu_\pi(\sigma, I) + \mu_\nu(\sigma, I)], \quad (1)$$

with $\mu_\tau(\sigma, I)$ being the magnetic moment of a state (σ, I)

$$\begin{aligned} \mu_\tau(\sigma, I) &= \langle \Psi_{II}^\sigma | \hat{\mu}_z^\tau | \Psi_{II}^\sigma \rangle \\ &= \frac{I}{\sqrt{I(I+1)}} \langle \Psi_I^\sigma | \hat{\mu}^\tau | \Psi_I^\sigma \rangle \\ &= \frac{I}{\sqrt{I(I+1)}} \left[g_l^\tau \langle \Psi_I^\sigma | \hat{j}^\tau | \Psi_I^\sigma \rangle + (g_s^\tau - g_l^\tau) \langle \Psi_I^\sigma | \hat{s}^\tau | \Psi_I^\sigma \rangle \right], \end{aligned} \quad (2)$$

where $\tau = \pi$ and ν for protons and neutrons, respectively.

The TPSM constructs the shell-model space by using the axially asymmetric Nilsson single-particle states with a quadrupole deformation ϵ_2 and triaxial deformation ϵ' . Pairing correlations are incorporated into the Nilsson states by the BCS calculations. The consequence of the Nilsson-BCS calculations defines a quasiparticle (qp) vacuum $|\Phi(\epsilon_2, \epsilon')\rangle \equiv |\Phi\rangle$ and the associated set of qp states in the intrinsic frame. Angular momentum projection [16] transforms the wave-functions from the intrinsic frame to the laboratory frame. The TPSM wave-function is generally written as

$$|\Psi_{IM}^\sigma\rangle = \sum_K f_{IK}^\sigma \hat{P}_{MK}^I |\Phi\rangle. \quad (3)$$

Thus, a state with good angular momentum is obtained as a linear combination of angular-momentum-projected Nilsson-BCS states. In Eq. (3), σ specifies the states with the same angular momentum I , \hat{P}_{MK}^I is the angular-momentum-projection operator [16]

$$\hat{P}_{MK}^I = \frac{2I+1}{8\pi^2} \int d\Omega D_{MK}^I(\Omega) \hat{R}(\Omega), \quad (4)$$

and $|\Phi\rangle$ represents the triaxial qp vacuum state

$$\left\{ \hat{P}_{MK}^I |\Phi\rangle, 0 \leq K \leq I \right\}. \quad (5)$$

For studying the low-spin states with $0 \leq I \leq 10$ before any quasi-particle alignment may occur, this is the simplest possible configuration space for an even-even nucleus with the γ -degree of freedom included. As in the earlier calculations [14, 15], we use the pairing plus quadrupole-quadrupole (QQ) Hamiltonian with inclusion of the quadrupole-pairing term

$$\hat{H} = \hat{H}_0 - \frac{1}{2} \chi \sum_\mu \hat{Q}_\mu^\dagger \hat{Q}_\mu - G_M \hat{P}^\dagger \hat{P} - G_Q \sum_\mu \hat{P}_\mu^\dagger \hat{P}_\mu. \quad (6)$$

The corresponding triaxial Nilsson Hamiltonian is given by

$$\hat{H}_N = \hat{H}_0 - \frac{2}{3} \hbar \omega \left(\epsilon_2 \hat{Q}_0 + \epsilon' \frac{\hat{Q}_{+2} + \hat{Q}_{-2}}{\sqrt{2}} \right). \quad (7)$$

In Eq. (6), \hat{H}_0 is the spherical single-particle Hamiltonian, which contains a proper spin-orbit force [20]. The axial and triaxial terms of the Nilsson potential in Eq. (7) contain the parameters ϵ_2 and ϵ' , respectively, which are related

TABLE I: The quadrupole and triaxial deformation parameters with which the deformed bases are constructed.

Z = 64	^{152}Gd	^{154}Gd	^{156}Gd	^{158}Gd	^{160}Gd					
ϵ_2	0.212	0.278	0.295	0.305	0.320					
ϵ'	0.115	0.115	0.105	0.105	0.115					
Z = 66	^{154}Dy	^{156}Dy	^{158}Dy	^{160}Dy	^{162}Dy	^{164}Dy				
ϵ_2	0.210	0.240	0.260	0.270	0.280	0.290				
ϵ'	0.120	0.130	0.120	0.125	0.130	0.140				
Z = 68	^{156}Er	^{158}Er	^{160}Er	^{162}Er	^{164}Er	^{166}Er	^{168}Er	^{170}Er		
ϵ_2	0.200	0.230	0.257	0.265	0.258	0.267	0.273	0.272		
ϵ'	0.125	0.125	0.125	0.125	0.130	0.135	0.125	0.110		
Z = 70	^{164}Yb	^{166}Yb	^{168}Yb	^{170}Yb	^{172}Yb	^{174}Yb	^{176}Yb			
ϵ_2	0.260	0.253	0.265	0.280	0.292	0.295	0.285			
ϵ'	0.110	0.120	0.115	0.110	0.095	0.095	0.100			
Z = 72	^{166}Hf	^{168}Hf	^{170}Hf	^{172}Hf	^{174}Hf	^{176}Hf	^{178}Hf	^{180}Hf		
ϵ_2	0.231	0.240	0.250	0.260	0.270	0.285	0.280	0.275		
ϵ'	0.120	0.120	0.115	0.105	0.100	0.100	0.100	0.095		
Z = 74	^{168}W	^{170}W	^{172}W	^{174}W	^{176}W	^{178}W	^{180}W	^{182}W	^{184}W	^{186}W
ϵ_2	0.193	0.201	0.217	0.216	0.210	0.201	0.195	0.195	0.190	0.186
ϵ'	0.095	0.110	0.110	0.105	0.110	0.095	0.095	0.085	0.095	0.080
Z = 76	^{178}Os	^{180}Os	^{182}Os	^{184}Os	^{186}Os	^{188}Os	^{190}Os	^{192}Os		
ϵ_2	0.188	0.178	0.170	0.173	0.163	0.154	0.139	0.138		
ϵ'	0.110	0.100	0.100	0.095	0.105	0.105	0.100	0.090		
Z = 78	^{182}Pt	^{184}Pt	^{186}Pt	^{188}Pt	^{190}Pt	^{192}Pt	^{194}Pt	^{196}Pt	^{198}Pt	
ϵ_2	0.187	0.192	0.168	0.130	0.128	0.120	0.113	0.160	0.167	
ϵ'	0.110	0.115	0.115	0.105	0.100	0.090	0.080	0.070	0.060	

to the γ deformation parameter by $\gamma = \arctan(\epsilon'/\epsilon_2)$. The QQ -force strength χ is adjusted such that the quadrupole deformation ϵ_2 is obtained as a result of the self-consistent mean-field HFB calculation [16]. The monopole pairing strength G_M is of the standard form $G_M = [20.12 \mp 13.13(N - Z)/A]/A$, with “-” for neutrons and “+” for protons, which approximately reproduces the observed odd-even mass differences in this mass region. The quadrupole pairing strength G_Q is assumed to be proportional to G_M , the proportionality constant being fixed as usual to be 0.16 for all nuclei considered in this paper. ϵ' in Eq. (7) can be adjusted, reflecting how much the system is γ -deformed. As valence single-particle space, we have included three major shells, $N = 4, 5, 6$ (3,4,5), for neutrons (protons).

In short, the philosophy of the present approach is that based on a deformed Nilsson potential, one performs explicit angular-momentum projection with a two-body interaction which conforms (through self-consistent conditions) with the mean-field Nilsson potential. The Hamiltonian with separable forces serves only as an effective interaction, the strengths of which have been fitted to the experimental data. The Hamiltonian in Eq. (6) is diagonalized using the projected basis of Eq. (5). We emphasize two quantum-mechanical features of this kind of approach, both of which are actually of the shell-model character. First, it should be noted that, although only the qp-vacuum state is included in the basis, its triaxial nature generates the K -mixing when the diagonalization is carried out. The expansion coefficients f , obtained through the diagonalization of the shell-model Hamiltonian, describe the amount of K -mixing and specify various physical states (e.g. g-, γ -, $\gamma\gamma$ -bands, \dots) [17]. Second, the deformed single-particle states with deformation parameters ϵ_2 and ϵ' are used solely as a starting basis. It is sufficient to have these deformation parameters close to those obtained by the mean-field calculations or to those experimentally adopted values. Of course, a large departure from a “true” deformation would result in a significant enhancement in dimension of the configuration space, with the extreme case being the conventional shell model based on a spherical basis ($\epsilon_2 = \epsilon' \equiv 0$).

III. RESULTS AND DISCUSSION

We have calculated 61 nuclei from the Gd, Dy, Er, Yb, Hf, W, Os, and Pt isotopic chains. This large group includes nuclei with very different collective behavior. It is well-known that in the light mass region with neutron number around 90, nuclei are soft against triaxiality, and the nuclei are traditionally known as γ -soft nuclei. On the other hand, the heavier isotopes in the Os and Pt chains contain also significant γ -softness, and these are typical examples of $O(6)$ nuclei according to the interacting boson model [21]. Between these two regions, nuclei are strongly deformed, for most of which the deformation is axial and the low-lying spectrum typically exhibits a regular rotor behavior. In

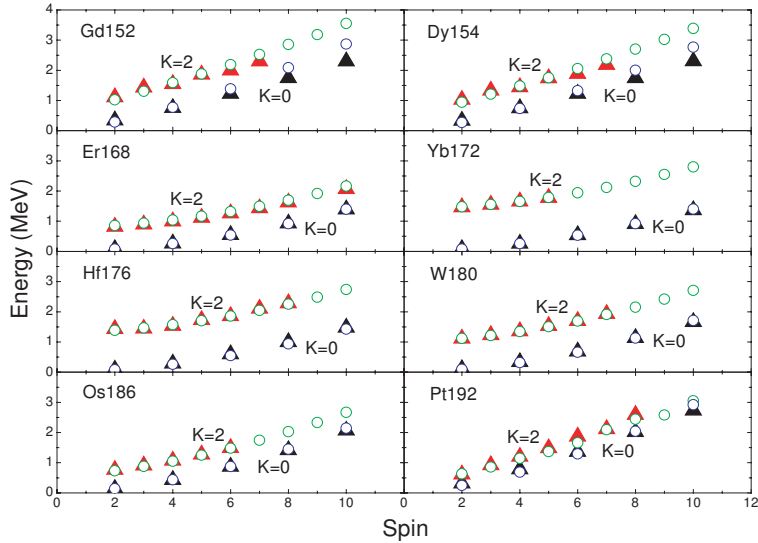


FIG. 1: (Color online) Comparison of calculated energies with experimental data for g-bands ($K = 0$) and γ -bands ($K = 2$). Open circles represent the calculated results and solid triangles the data.

Table I, we list the deformation parameters with which the deformed bases are constructed. The listed quadrupole deformations ϵ_2 are similar to the theoretical values known in the literature [22] and have also a consistent isotopic trend with that of the experimentally adopted ones [23]. In the calculation, we treat ϵ' as a free parameter, adjusted to reproduce the excitations of the γ -band relative to the g-band. However, once an ϵ' is chosen to best reproduce the g- and γ -bands, it sets a strict constraint in the g factor calculations.

Fig. 1 shows the calculated energy levels together with experimental data for g-bands and γ -bands. We include in the figure only one nucleus selected from each of the isotopic chains because all the calculations have achieved the same level of agreement. These examples are chosen to represent nuclei with distinct collective behavior. For instance, with neutron number 88, ^{152}Gd and ^{154}Dy are typical γ -soft nuclei lying in the transitional region of the light rare earth. It was demonstrated [15] that a microscopic description of the changing moment of inertia with angular momentum (i.e. the slope of the curves in Fig. 1) is possible only if triaxiality is introduced into the deformed basis. ^{168}Er , ^{172}Yb , and ^{176}Hf are representative examples of strongly deformed nuclei lying in the midshell, which have nearly constant moment of inertia. To describe the Yrast properties of these nuclei, it is normally sufficient to employ the axial PSM [16]. Nevertheless, it was shown in Ref. [17] that inclusion of triaxiality in the basis does not affect the description of the Yrast band. It can however simultaneously reproduce multi-phonon γ -bands. Finally, ^{186}Os and ^{192}Pt are again γ -soft in the transitional region, which exhibit very low-lying γ bands. For all these nuclei with very different rotational behavior, it can be seen from Fig. 1 that the energy levels have been equally well reproduced by the TPSM.

The wave-functions are used to evaluate the magnetic dipole moment and the g factor can then be obtained. In the angular-momentum projection theory, the reduced matrix element for an operator \hat{m} (with \hat{m} being either \hat{j} or \hat{s} in Eq. (2)) can be explicitly expressed as

$$\begin{aligned} \langle \Psi_I^\sigma | \hat{m}^\tau | \Psi_I^\sigma \rangle &= \sum_{K_i, K_f} f_{IK_i}^\sigma f_{IK_f}^\sigma \sum_{M_i, M_f, M} (-)^{I-M_f} \begin{pmatrix} I & 1 & I \\ -M_f & M & M_i \end{pmatrix} \langle \Phi | \hat{P}_{K_f M_f}^I \hat{m}_{1M} \hat{P}_{K_i M_i}^I | \Phi \rangle \\ &= (2I+1) \sum_{K_i, K_f} (-)^{I-K_f} f_{IK_i}^\sigma f_{IK_f}^\sigma \sum_{M', M''} \begin{pmatrix} I & 1 & I \\ -K_f & M' & M'' \end{pmatrix} \\ &\quad \times \int d\Omega D_{M'' K_i}(\Omega) \langle \Phi | \hat{m}_{1M'} \hat{R}(\Omega) | \Phi \rangle. \end{aligned}$$

In our calculations, the following standard values for g_l and g_s appearing in Eq. (2) have been taken

$$\begin{aligned} g_l^\pi &= 1, & g_s^\pi &= 5.586 \times 0.75, \\ g_l^\nu &= 0, & g_s^\nu &= -3.826 \times 0.75. \end{aligned}$$

g_s^π and g_s^ν are damped by a usual 0.75 factor from the free-nucleon values to account for the core-polarization and

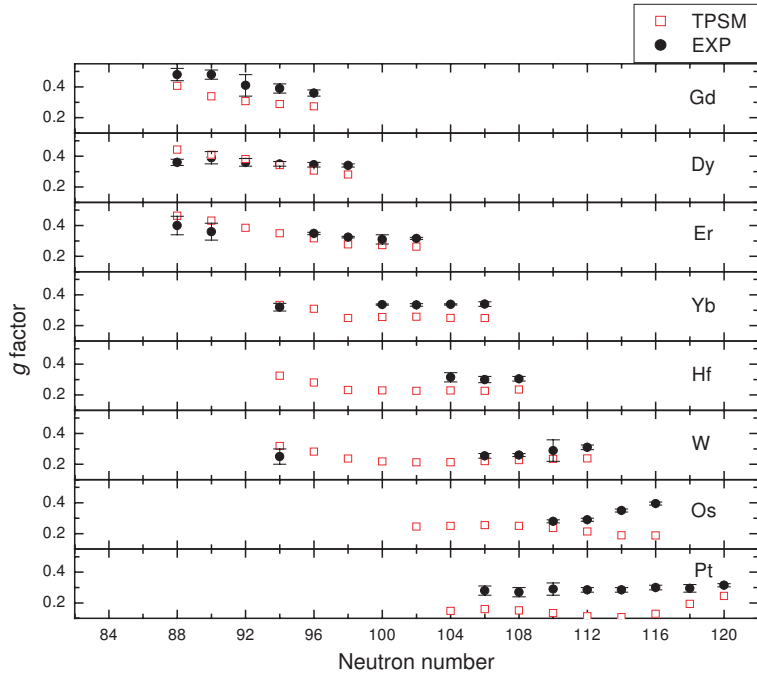


FIG. 2: (Color online.) Comparison of calculated 2^+ state g factors with available data.

meson-exchange current corrections [24]. These same values are used for all g factor calculations in the present paper, as in the previous projected shell model calculations, without any adjustment for individual nuclei.

We now present the systematics of g factor of first 2^+ state for all the isotopic chains from Gd to Pt. In Fig. 2, a comparison of calculated results with available data [1, 2, 3] is given. Several interesting trends are clearly observed. The experimental $g(2_1^+)$ values of Gd, Dy, and Er isotopes show a down-sloping trend with increasing neutron number N ; those of W and Os isotopes exhibit an up-sloping behavior; and, according to the current set of data, the g factors of Yb, Hf and Pt isotopes are almost constant within each isotopic chain. From Fig. 2 it can be seen that the observed trends for all the isotopic chains from Gd to W are correctly reproduced by the present calculations. Especially for the Dy, Er, and W nuclei, the agreement with data is nearly perfect. The down-sloping trend of Gd, Dy, and Er isotopes is well described. The calculation further predicts that for the Yb, Hf, and W isotopic chains, a down-sloping trend is still visible with $N \leq 100$, but becomes nearly constant at the neutron midshell. The up-sloping trend of W isotopes with $N \geq 106$ is well reproduced by the calculation.

While the calculation predicts a flat behavior of $g(2_1^+)$ for the lighter Os nuclei till $N = 110$, a clear departure from data occurs for heavier Os isotopes and for all the Pt isotopes considered in this paper. Moreover, for the Pt isotopes, the trend of the theoretical $g(2_1^+)$ first decreases from $N = 106$ to 112, and then increases from $N = 114$ to 120, which is not supported by the flat behavior of $g(2_1^+)$ found in the experiment data. Although for ^{196}Pt and ^{198}Pt , the theoretical values become closer to the data, we must conclude that the present calculation fails to give the observed $g(2_1^+)$ trend for the Os and Pt chains. We have tried various calculations by constructing our deformed model space with different (ϵ_2, ϵ') deformations. In the example of ^{192}Pt , it is found that as deformations increase, the g factor values start going up. With $\epsilon_2 = 0.28$ and $\epsilon' = 0.25$, a much greater value ($g = 0.315$), which approaches the experimental data, can be obtained. However, the energy levels in this nucleus cannot be simultaneously described within a basis built with such large deformations.

The failure appears to be unexpected because in the light Gd, Dy, and Er region with $N \approx 90$, where nuclei are also transitional with γ -softness, $g(2_1^+)$ can be well reproduced by the present calculation. This may indicate that, although both g - and γ -band energies in the Os and Pt chains are reproduced by the model, the obtained wave-functions can be very wrong. This poses an interesting question that the same model with triaxiality constructed in it does not describe equally well the two γ -soft, transitional regions in the rare earth.

Triaxiality has been one of the most interesting subjects in nuclear structure. It determines the shape of the nuclear surface, which is nevertheless not a directly measurable quantity. Traditionally, there have two physical pictures for triaxiality. The γ -unstable picture of Wilets and Jean [25] assumes that the nucleus is soft with respect to the triaxial shape and the wave-function is described over a range of γ variable, whereas the rigid-triaxial-rotor picture of Davydov and Filippov [26] suggests a stable triaxial deformation, with the wave function peaked at a finite γ . The

TPSM is constructed in a deformed basis with fixed quadrupole deformation ϵ_2 and triaxial deformation ϵ' . It is a microscopic model but the corresponding classical picture is close to that of Davydov and Filippov [26]. Otsuka and Sugita proposed an ansatz [27] of equivalence between γ instability and rigid triaxiality. They suggested a relationship between the two pictures such that a γ -unstable state can be generated from the rigid triaxial intrinsic state with $\gamma = 30^\circ$. Now if we apply the relation $\gamma = \arctan(\epsilon'/\epsilon_2)$ for the deformation parameters listed in Table I, we indeed find that our γ lie in the range of 20° to 40° . Thus it seems that in our microscopic calculations, a γ deformation around 30° is necessary to reproduce the energy levels of γ -soft nuclei [15, 17]. This is in a support of the Otsuka-Sugita ansatz. However, the wave-functions given by the two pictures are certainly not expected to be even close, and g factor is just a sensitive probe of wave-functions. Our microscopic study thus suggests that the Otsuka-Sugita ansatz may not apply to the γ -soft region of the heavier Os and Pt region as far as wave-function is concerned.

This calls for a further improvement of the projected shell model type approaches to generally describe transitional nuclei. More correlations need to be included. These correlations can be introduced by addition of the D-pair operators to the vacuum state [28], which takes both quasiparticle and collective degrees of freedom explicitly into account in a shell model basis. Generator coordinate method, which consists of a construction of a linear superposition of different product wave-functions, can also be adopted. Currently, we are working on adding multi-quasi-particle states on top of the triaxially deformed vacuum state. Results along these lines will be reported elsewhere.

IV. SUMMARY

Inspired by the recent experimental work of Berant *et al.*, [1], we have made an attempt to study systematically $g(2^+)$ for all the isotopes from Gd to Pt, using the newly developed triaxial projected shell model approach. With a single set of interaction strengths, we have carried out shell model diagonalizations for each nucleus in a projected basis constructed with appropriate deformations. We have been able to reproduce remarkably well the low-lying g - and γ -band for all the nuclei considered in the paper. With the same set of calculation conditions that reproduce the energy levels, we have calculated g factors of first 2^+ state for each nucleus. We have found that for the isotopes from the Gd to W chain, the characteristics of experimental data along an isotopic chain are well reproduced by the theoretical calculations, such as the downsloping trend in the Gd, Dy, and Er isotopes, the upsloping trend in the W isotopes, and the flat behavior of the Yb and Hf isotopes. For the heavier Os and Pt nuclei, we have found that although the energy levels can be described equally well as in the lighter nuclei, the calculated g factors are wrong, implying deficiency in the wave-functions.

With fixed quadrupole deformation ϵ_2 and triaxial deformation ϵ' in the starting basis, the triaxial projected shell model may have the classical picture of Davydov and Filippov [26]. According to the Otsuka-Sugita ansatz [27], our model should apply to the γ -soft systems if the deformed basis has $\gamma \approx 30^\circ$. The applicability of our model to the collective γ -vibrational states for the light and midshell rare earth nuclei [17] seems to support the Otsuka-Sugita ansatz. However, the current work on the systematics of g factor, which reflects detailed structure of wave-functions, may have suggested that the Otsuka-Sugita ansatz does not apply to the other end of the shell in the heavier Os and Pt region.

V. ACKNOWLEDGMENTS

Communication with Professor J.-y. Zhang is acknowledged. Y.S. thanks the colleagues at the Physics Departments of Xuzhou Normal University and Tsinghua University for warm hospitality extended to him. This work is partly supported by NSF under contract PHY-0140324, and by the China NNSF with grant 10325521.

[1] Z. Berant, A. Wolf, N. V. Zamfir, M. A. Caprio, D. S. Brenner, N. Pietralla, R. L. Gill, R. F. Casten, C. W. Beausang, R. Krücken, C. J. Barton, J. R. Cooper, A. A. Hecht, D. M. Johnson, J. R. Novak, H. Cheng, B. F. Albanna, and G. Gurdal, Phys. Rev. C **69**, 034320 (2004).

[2] P. Raghavan, At. Data Nucl. Data Tables **42**, 189 (1989).

[3] N. J. Stone, Table of Nuclear Magnetic Dipole and Electric Quadrupole Moments, NNDC, <http://www.BNL.gov> (2001).

[4] W. Greiner, Nucl. Phys. **80**, 417 (1966).

[5] M. Sambataro, O. Scholten, A. E. L. Dieperink, and G. Piccito, Nucl. Phys. **A 423**, 333 (1984).

[6] B. A. Brown, N. J. Stone, J. R. Stone, I. S. Towner, and M. Hjorth-Jensen, Phys. Rev. C, in press.

[7] K. Sugawara-Tanabe and K. Tanabe, Phys. Lett. B **207**, 243 (1988).

[8] A. Ansari, Phys. Rev. C **41**, 782 (1990).

- [9] M. L. Cescato, Y. Sun, and P. Ring, Nucl. Phys. **A 533**, 455 (1991).
- [10] M. Saha and S. Sen, Nucl. Phys. **A 552**, 37 (1993).
- [11] Y. Sun and J. L. Egido, Nucl. Phys. **A 580**, 1 (1994).
- [12] V. Velazquez, J. Hirsch, Y. Sun, and M. Guidry, Nucl. Phys. **A 653**, 355 (1999).
- [13] Y. Sun, J.-y. Zhang, and M. Guidry, Phys. Rev. C **63**, 047306 (2001).
- [14] Y. Sun, J. A. Sheikh, and G.L. Long, Phys. Lett. **B 533**, 253 (2002).
- [15] J. A. Sheikh and K. Hara, Phys. Rev. Lett. **82**, 3968 (1999).
- [16] K. Hara and Y. Sun, Int. J. Mod. Phys. **E 4**, 637 (1995).
- [17] Y. Sun, K. Hara, J. A. Sheikh, J. Hirsch, V. Velazquez, and M. Guidry, Phys. Rev. C **61**, 064323 (2000).
- [18] J. A. Sheikh, Y. Sun, and R. Palit, Phys. Lett. **B 507**, 115 (2001).
- [19] P. Boutachkov, A. Aprahamian, Y. Sun, J. A. Sheikh, and S. Frauendorf, Eur. Phys. J. **A 15**, 455 (2002).
- [20] S. G. Nilsson *et al.*, Nucl. Phys. A **131** (1969) 1.
- [21] F. Iachello and A. Arima, *The Interacting Boson Model* (Cambridge University Press, Cambridge, 1987).
- [22] P. Möller, J. R. Nix, W. D. Myers, and W. J. Swiatecki, At. Data Nucl. Data Tables, **59**, 185 (1995).
- [23] S. Raman, C. W. Nestor, Jr., and P. Tikkanen, At. Data Nucl. Data Tables, **78**, 1 (2001).
- [24] B. Castel and I. S. Towner, *Modern Theories of Nuclear Moments* (Clarendon, Oxford, 1990).
- [25] L. Wilets and M. Jean, Phys. Rev. **102**, 788 (1956).
- [26] A. S. Davydov and G. F. Filippov, Nucl. Phys. **8**, 237 (1958).
- [27] T. Otsuka and M. Sugita, Phys. Rev. Lett. **59**, 1541 (1987).
- [28] Y. Sun and C.-L. Wu, Phys. Rev. C **68**, 024315 (2003).